

# Low-frequency $K^\pi = 0^+$ modes in deformed neutron-rich nuclei: Pairing- and $\beta$ -vibrational modes of neutron

Kenichi Yoshida

*Department of Physics, Graduate School of Science, Kyoto University, Kyoto 606-8502, Japan*

Masayuki Yamagami

*Nishina Center for Accelerator Based Science, The Institute of Physical and Chemical Research (RIKEN), Wako, Saitama 351-0198, Japan*

(Dated: September 15, 2021)

Low-frequency  $K^\pi = 0^+$  states in deformed neutron-rich nuclei are investigated by means of the quasiparticle-random-phase approximation based on the Hartree-Fock-Bogoliubov formalism in the coordinate space. We have obtained the very strongly collective  $K^\pi = 0^+$  modes not only in neutron-rich Mg isotope but also in Cr and Fe isotopes in  $N = 40$  region, where the onset of nuclear deformation has been discussed. It is found that the spatially extended structure of neutron quasiparticle wave functions around the Fermi level brings about a striking enhancement of the transition strengths. It is also found that the fluctuation of the pairing field plays an important role in generating coherence among two-quasiparticle excitations of neutron.

PACS numbers: 21.10.Re; 21.60.Ev; 21.60.Jz

## I. INTRODUCTION

Physics of nuclei far from  $\beta$ -stability has been one of the main current subjects of nuclear physics. Quest for new kinds of collective motion in exotic unstable nuclei is one of the most interesting issues in nuclear structure physics and has been actively studied both experimentally and theoretically [1]. Because low-lying collective excitations are sensitive to the shell structure around the Fermi level, one can expect unique excitation modes to emerge associated with the new spatial structures such as neutron skins and novel shell structures which generate new regions of deformation.

Breaking of the spherical magic number  $N = 20, 28$  and striking enhancement of  $B(E2; 0_1^+ \rightarrow 2_1^+)$  in Mg isotopes towards drip line are under lively discussions in connection with onset of the quadrupole deformation and continuum coupling [2, 3, 4, 5, 6, 7, 8, 9, 10, 11, 12]. Furthermore in heavier mass region, collectivities and breaking of the  $N = 40$  sub-shell have been recently discussed for neutron-rich Cr and Fe isotopes [15, 16, 17, 18, 19]. Although many investigations based on the random phase approximation (RPA) or the Quasiparticle RPA (QRPA) including the pairing correlations [20, 21, 22, 23, 24, 25, 26, 27, 28, 29, 30, 31, 32, 33, 34, 35, 36, 37, 38] on multipole responses of neutron-rich nuclei have been done, they are largely restricted to spherical systems.

Recently, low-lying RPA modes in deformed neutron-rich nuclei have been investigated by several groups [39, 40, 41, 42, 43, 44, 45, 46, 47, 48, 49]. These calculations, however, do not take into account the pairing correlation, or rely on the BCS pairing (except for Ref. [46] and our very recent investigation [49]), which is inappropriate for describing the pairing correlation in drip line nuclei due to the unphysical nucleon gas problem [50].

In Ref. [51], we constructed a new computer code that carries out the deformed QRPA calculation based

on the coordinate-space Hartree-Fock-Bogoliubov (HFB) formalism, and investigated quadrupole excitations in neutron-rich Mg isotopes close to the drip line around  $N = 28$ . We obtained low-lying  $K^\pi = 0^+$  and  $2^+$  quadrupole excitation modes in  $^{36,38,40}\text{Mg}$ . We found that the  $K^\pi = 0^+$  mode in  $^{40}\text{Mg}$  was generated by coherent superposition of neutron two-quasiparticle (2qp) excitations in loosely bound and resonant states. Among them, the neutron 2qp excitations of up-sloping oblate levels and down-sloping prolate levels play the major role. A deformed gap is formed at  $N = 28$  around  $\beta_2 = 0.3$  [12] due to the crossings between the up-sloping  $\nu[303]7/2$  level and the down-sloping  $\nu[310]1/2$  level, and this deformed closed shell approximately corresponds to the  $(f_{7/2})^{-2}(p_{3/2})^2$  configuration in the spherical shell model representation [9] (see Fig. 1). It was also found that the dynamical pairing correlation, *i.e.*, fluctuation of the pairing field played a crucial role in generating coherence among neutron 2qp excitations.

The single-particle levels which are  $(2j + 1)$ -fold degenerate in the spherical potential are split by the nuclear deformation to 2-fold degenerate levels with the single-particle energy to first order of  $\beta_2$  as [13]

$$\sim \beta_2 \frac{3\Omega^2 - j(j+1)}{j(j+1)}. \quad (1)$$

In a prolately deformed potential ( $\beta_2 > 0$ ), a level with small value of  $\Omega$  ( $z$ -component of the angular momentum  $j$ ) has a negative slope. We call this single-particle level a down-sloping prolate level in this paper, and refer a positive slope level with large  $\Omega$  as a up-sloping oblate level.

Because the deformed shell gap is, in many cases, made by the up-sloping and the down-sloping levels [14], we investigate in this paper detailed and systematic properties of low-frequency  $K^\pi = 0^+$  modes in deformed neutron-rich Mg, Cr and Fe isotopes, and discuss generic features

of the soft  $K^\pi = 0^+$  modes uniquely appeared in deformed neutron-rich nuclei.

The paper is organized as follows. In the next section, we present our model of the deformed HFB and QRPA. Numerical results and discussion are given in § III. Finally, we summarize the paper in § IV.

## II. MODEL

We briefly summarize our approach (see Ref. [51] for details). In order to discuss simultaneously effects of nuclear deformation and pairing correlations including the continuum, we solve the HFB equations [50, 52, 53]

$$\begin{pmatrix} h^\tau(\mathbf{r}\sigma) - \lambda^\tau & \tilde{h}^\tau(\mathbf{r}\sigma) \\ \tilde{h}^\tau(\mathbf{r}\sigma) & -(h^\tau(\mathbf{r}\sigma) - \lambda^\tau) \end{pmatrix} \begin{pmatrix} \varphi_{1,\alpha}^\tau(\mathbf{r}\sigma) \\ \varphi_{2,\alpha}^\tau(\mathbf{r}\sigma) \end{pmatrix} = E_\alpha \begin{pmatrix} \varphi_{1,\alpha}^\tau(\mathbf{r}\sigma) \\ \varphi_{2,\alpha}^\tau(\mathbf{r}\sigma) \end{pmatrix} \quad (2)$$

directly in the cylindrical-coordinates assuming axial and reflection symmetries. Here  $\tau = \nu$  (neutron) and  $\pi$  (proton), and  $\mathbf{r} = (\rho, z, \phi)$ . For the mean-field Hamiltonian  $h$ , we employ the deformed Woods-Saxon potential with the parameters used in Ref. [51] for  $^{34}\text{Mg}$  and those in Ref. [39] for neutron-rich Cr and Fe isotopes. The pairing field is treated self-consistently by using the density-dependent contact interaction [54, 55],

$$v_{pp}(\mathbf{r}, \mathbf{r}') = V_0 \frac{1 - P_\sigma}{2} \left[ 1 - \frac{\varrho^{\text{IS}}(\mathbf{r})}{\varrho_0} \right] \delta(\mathbf{r} - \mathbf{r}'). \quad (3)$$

with  $\varrho_0 = 0.16 \text{ fm}^{-3}$ . Here  $\varrho^{\text{IS}}(\mathbf{r})$  denotes the isoscalar density and  $P_\sigma$  the spin exchange operator. Because the time-reversal symmetry and the reflection symmetry with respect to the  $x - y$  plane are assumed, we have only to solve for positive  $\Omega$  and positive  $z$ . We use the lattice mesh size  $\Delta\rho = \Delta z = 0.8 \text{ fm}$  and the box boundary condition at  $\rho_{\text{max}} = 10.0 \text{ fm}$  and  $z_{\text{max}} = 12.8 \text{ fm}$ . The quasiparticle energy is cut off at 50 MeV and the quasiparticle states up to  $\Omega^\pi = 15/2^\pm$  are included.

Using the quasiparticle basis obtained by solving the HFB equation (2), we solve the QRPA equation in the matrix formulation [56]

$$\sum_{\gamma\delta} \begin{pmatrix} A_{\alpha\beta\gamma\delta} & B_{\alpha\beta\gamma\delta} \\ B_{\alpha\beta\gamma\delta} & A_{\alpha\beta\gamma\delta} \end{pmatrix} \begin{pmatrix} f_{\gamma\delta}^\lambda \\ g_{\gamma\delta}^\lambda \end{pmatrix} = \hbar\omega_\lambda \begin{pmatrix} 1 & 0 \\ 0 & -1 \end{pmatrix} \begin{pmatrix} f_{\alpha\beta}^\lambda \\ g_{\alpha\beta}^\lambda \end{pmatrix}. \quad (4)$$

The residual interaction in the particle-particle (p-p) channel appearing in the QRPA matrices  $A$  and  $B$  is the density-dependent contact interaction (3). On the other hand, for the residual interaction in the particle-hole (p-h) channel, we use the Skyrme-type interaction

$$v_{ph}(\mathbf{r}, \mathbf{r}') = \left[ t_0(1 + x_0 P_\sigma) + \frac{t_3}{6}(1 + x_3 P_\sigma) \varrho^{\text{IS}}(\mathbf{r}) \right] \delta(\mathbf{r} - \mathbf{r}'), \quad (5)$$

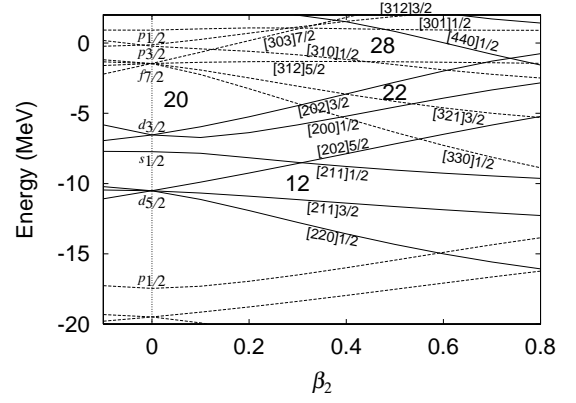


FIG. 1: Single-particle energies in the deformed WS potential for neutrons in  $^{40}\text{Mg}$ , plotted as functions of the quadrupole deformation parameter  $\beta_2$ . Solid and dotted lines denote positive- and negative-parity levels, respectively. Single-particle levels are labeled with the asymptotic quantum numbers  $[N n_3 \Lambda] \Omega$ .

with  $t_0 = -1100 \text{ MeV}\cdot\text{fm}^3$ ,  $t_3 = 16000 \text{ MeV}\cdot\text{fm}^6$ ,  $x_0 = 0.5$ , and  $x_3 = 1.0$  [57]. Because the deformed Woods-Saxon potential is used for the mean field, we renormalize the residual interaction in the p-h channel by multiplying a factor  $f_{ph}$  to get the spurious  $K^\pi = 1^+$  mode (representing the rotational mode) at zero energy ( $v_{ph} \rightarrow f_{ph} \cdot v_{ph}$ ). We cut the 2qp space at  $E_\alpha + E_\beta \leq 30 \text{ MeV}$  due to the excessively demanding computer memory for the model space consistent with that adopted in the HFB calculation. Accordingly, we need another factor  $f_{pp}$  for the p-p channel. We determine this factor such that the spurious  $K^\pi = 0^+$  mode associated with the particle number fluctuation appears at zero energy ( $v_{pp} \rightarrow f_{pp} \cdot v_{pp}$ ). The dimension of the QRPA equation (4) is 2512 for  $^{34}\text{Mg}$  and 3804 for  $^{72}\text{Fe}$ . Within this model space, the energy-weighted sum rule for the quadrupole  $K^\pi = 0^+$  excitation is satisfied 92.9% for  $^{34}\text{Mg}$  and 97.0% for  $^{72}\text{Fe}$ .

## III. RESULTS AND DISCUSSION

Let us now discuss the low-frequency  $K^\pi = 0^+$  modes in  $^{34}\text{Mg}$  in § III A and in neutron-rich Cr and Fe isotopes with  $N \simeq 40$  in § III B.

### A. $^{34}\text{Mg}$

Figure 1 shows the single-particle energy diagram for the WS potential as a function of deformation parameter  $\beta_2$ . At around  $\beta_2 = 0.5$ , the deformed shell gap is formed at  $N = 22$  due to the crossings between the up-sloping  $\nu[202]3/2$  and the down-sloping  $\nu[330]1/2$  and  $\nu[321]3/2$  levels. In Fig. 2, we show the low-lying excitation spectrum below 3 MeV in  $^{34}\text{Mg}$ . Here excitation energies are

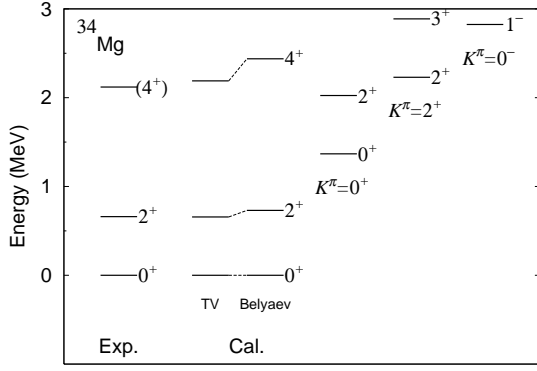


FIG. 2: Excitation energy spectrum in  $^{34}\text{Mg}$  obtained by the QRPA calculation using  $\beta_2 = 0.4$  and  $V_0 = -400 \text{ MeV}\cdot\text{fm}^3$  and available experimental data [4].

evaluated by [58]

$$E(I, K) = \hbar\omega_{\text{RPA}} + \frac{\hbar^2}{2\mathcal{J}_{\text{TV}}}(I(I+1) - K^2), \quad (6)$$

with the vibrational frequencies,  $\omega_{\text{RPA}}$ , and the Thouless-Valatin moment of inertia,  $\mathcal{J}_{\text{TV}}$ , calculated by the QRPA. The pairing strength  $V_0$  for  $^{34}\text{Mg}$  is determined in order to reproduce the experimental excitation energy of  $E(2_1^+) = 660 \text{ keV}$  [4]. In this figure, we also show the excitation energies evaluated by using the Belyaev moment of inertia,  $\mathcal{J}_{\text{Belyaev}}$ , where the residual interaction is turned off. We found that  $\mathcal{J}_{\text{TV}}$  becomes about 11% larger than  $\mathcal{J}_{\text{Belyaev}}$  due to the time-odd component in the residual interactions of (3) and (5). The  $K^\pi = 2^+$  mode at 2.01 MeV is dominantly generated by the proton p-h excitations as that in  $^{36,38,40}\text{Mg}$  [51]; these are proton dominated  $\gamma$ -vibrational modes. The negative parity  $K^\pi = 0^-$  state at 2.61 MeV is mainly generated by the lowest neutron 2qp excitation of  $\nu[202]3/2 \otimes \nu[321]3/2$  with the excitation energy of 2.74 MeV. Its collectivity is thus rather weak.

The left panel of Fig. 3 shows the  $K^\pi = 0^+$  isoscalar quadrupole transition strengths, and the unperturbed 2qp transition strengths are shown in the lower panel. The intrinsic transition strength to the lowest  $K^\pi = 0^+$  excited state is about 43 Weisskopf units (1 W.u.  $\simeq 6.5 \text{ fm}^4$  for  $^{34}\text{Mg}$ ). This state is constructed by the coherent superposition of 2qp excitations of the up-sloping  $(\nu[202]3/2)^2$  and the down-sloping  $(\nu[330]1/2)^2$  and the  $(\nu[321]3/2)^2$  levels, together with the high-lying  $2\hbar\omega$  excitation of protons.

Generation mechanism of the soft  $K^\pi = 0^+$  mode in deformed neutron-rich nuclei is understood essentially by the schematic two-level model in Ref. [59]. They consider the case where only two  $\lambda\bar{\lambda}$  components are present in the wave functions both of the ground  $0_{\text{gs}}^+$  and of the excited

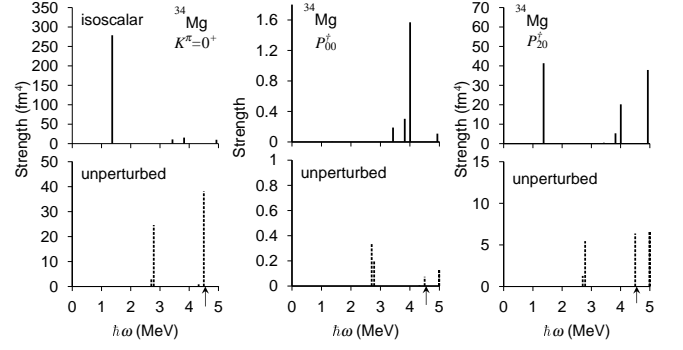


FIG. 3: QRPA strength distributions for the  $K^\pi = 0^+$  isoscalar quadrupole p-h excitations (left) and the monopole- and quadrupole-pair excitations (middle and right) in  $^{34}\text{Mg}$ , calculated using  $f_{ph} = 0.74$  and  $f_{pp} = 1.37$ . For comparison, unperturbed 2qp transition strengths are shown in the lower panels. The arrow indicates the neutron threshold energy  $E_{\text{th}} = 4.55 \text{ MeV}$  for 1qp continuum.

$0_2^+$  states;

$$|0_{\text{gs}}^+\rangle = \frac{a}{\sqrt{a^2 + b^2}}|\lambda_1\bar{\lambda}_1\rangle + \frac{b}{\sqrt{a^2 + b^2}}|\lambda_2\bar{\lambda}_2\rangle \quad (7a)$$

$$|0_2^+\rangle = -\frac{b}{\sqrt{a^2 + b^2}}|\lambda_1\bar{\lambda}_1\rangle + \frac{a}{\sqrt{a^2 + b^2}}|\lambda_2\bar{\lambda}_2\rangle. \quad (7b)$$

The transition matrix element for the quadrupole operator is then

$$\langle 0_{\text{gs}}^+|\hat{Q}_{20}|0_2^+\rangle = \frac{2ab}{a^2 + b^2}[\langle\lambda_1|\hat{Q}_{20}|\lambda_1\rangle - \langle\lambda_2|\hat{Q}_{20}|\lambda_2\rangle] \quad (8)$$

and it is proportional to the difference in the quadrupole moments of the individual orbitals composing the  $0^+$  states. In the case that the quadrupole moments of the orbitals have opposite signs to each other, this matrix element becomes large. This situation is realized in the level crossing region, where the up- and down-sloping orbitals exist. As the number of components increases in the QRPA calculations, the wave function becomes more complicated, and the transition matrix element reads (see Appendix B)

$$\langle K^\pi = 0^+|\hat{Q}_{20}|0\rangle = \sum_{\alpha\beta} Q_{20,\alpha\beta}^{(\text{uv})}(f_{\alpha\beta} + g_{\alpha\beta}) \equiv \sum_{\alpha\beta} M_{20,\alpha\beta}^{(\text{uv})}. \quad (9)$$

In the QRPA employing the separable interaction, for the major component of the QRPA eigenmode associated with the pairing fluctuation, the phase of the QRPA amplitudes,  $f_{\alpha\beta}$  and  $g_{\alpha\beta}$ , are opposite between particle-like levels and hole-like levels (due to the  $(u^2 - v^2)$  factor; see Appendix J of Ref. [60]). In the level crossing region, the particle-like level is the up-sloping oblate level, and the hole-like level is the down-sloping prolate level. Because the transition matrix elements for the QRPA eigenmodes are determined by the sum of products of the QRPA amplitudes and the individual 2qp transition

TABLE I: QRPA amplitudes for the  $K^\pi = 0^+$  state at 1.37 MeV in  $^{34}\text{Mg}$ . This mode has the proton strength  $B(E2) = 15.9e^2\text{fm}^4$ , the neutron strength  $B(Q^{\nu 2}) = 162\text{fm}^4$ , and the isoscalar strength  $B(Q^{\text{IS}2}) = 279\text{fm}^4$ , and the sum of backward-going amplitudes  $\sum |g_{\alpha\beta}|^2 = 0.141$ . The single-quasiparticle levels are labeled with the asymptotic quantum numbers  $[Nn_3\Lambda]\Omega$ . Only components with  $f_{\alpha\beta}^2 - g_{\alpha\beta}^2 > 0.01$  are listed.

$\alpha$	$\beta$	$E_\alpha + E_\beta$ (MeV)	$f_{\alpha\beta}$	$g_{\alpha\beta}$	$Q_{20,\alpha\beta}^{(\text{uv})}$ ( $\text{fm}^2$ )	$M_{20,\alpha\beta}^{(\text{uv})}$ ( $\text{fm}^2$ )	$P_{20,\alpha\beta}^{(\text{uu})}$ ( $\text{fm}^2$ )	$M_{20,\alpha\beta}^{(\text{add})}$ ( $\text{fm}^2$ )	$P_{00,\alpha\beta}^{(\text{uu})}$	$M_{00,\alpha\beta}^{(\text{add})}$
(a) $\nu[202]3/2$	$\nu[202]3/2$	2.70	-0.615	-0.230	-1.814	1.533	-1.128	0.864	0.579	-0.453
(b) $\nu[321]3/2$	$\nu[321]3/2$	2.79	0.688	0.052	4.962	3.673	2.335	1.745	0.443	0.334
(c) $\nu[330]1/2$	$\nu[330]1/2$	4.50	0.371	0.062	6.177	2.676	2.524	1.329	0.278	0.146

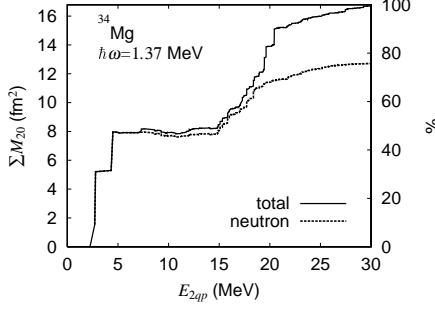


FIG. 4: Sum of the transition matrix element  $\sum_{\alpha\beta} M_{20,\alpha\beta}^{(\text{uv})}$  for the lowest  $K^\pi = 0^+$  state at 1.37 MeV. Solid and dotted lines denote the isoscalar and neutron transitions, respectively.

matrix elements in Eq. (9), they contribute coherently for the quadrupole transition.

In the present case, the main components generating the low-lying  $K^\pi = 0^+$  state are  $[202]3/2 \otimes [202]3/2$ ,  $[321]3/2 \otimes [321]3/2$  and  $[330]1/2 \otimes [330]1/2$ , which are the up-sloping and down-sloping levels with opposite quadrupole moments and the QRPA amplitudes have opposite signs as shown in Table I. Therefore, the strength for the quadrupole transition becomes enhanced. These three 2qp excitations contribute about 50 % of the total transition strength. Furthermore, many other 2qp excitations coherently participate to generate the lowest  $0^+$  state, which brings about further enhancement of the transition strength.

Figure 4 shows the partial sum of the transition matrix element for the  $K^\pi = 0^+$  mode  $\sum_{E_\alpha + E_\beta \leq E_{2qp}} M_{20,\alpha\beta}^{(\text{uv})}$  for the isoscalar and neutron excitations. We see that many 2qp excitations construct this state with coherence; each 2qp transition matrix element ( $M_{20,\alpha\beta}^{(\text{uv})}$ ) has a same sign. If the QRPA mode were a destructive state or a single 2qp excitation, the sum of the transition matrix element becomes zero in total or shows step function.

From this figure, we see another interesting feature: Soft  $K^\pi = 0^+$  mode in  $^{34}\text{Mg}$  is generated not only by neutron 2qp excitations around the Fermi level with the excitation energy around 5 MeV (three 2qp excitations discussed above) but also proton excitations

around 20 MeV. These proton excitations are  $2\hbar\omega$  excitations of giant resonance;  $\pi[211]3/2 \rightarrow \pi[431]3/2$  (19.5 MeV),  $\pi[101]3/2 \rightarrow \pi[321]3/2$  (17.3 MeV),  $\pi[110]1/2 \rightarrow \pi[330]1/2$  (19.6 MeV) and  $\pi[220]1/2 \rightarrow \pi[440]1/2$  (20.1 MeV). Due to this coupling with giant resonance of proton, the proton transition strength  $B(E2)$  is larger than that in  $^{40}\text{Mg}$ ;  $B(E2) = 15.9e^2\text{fm}^4$  in  $^{34}\text{Mg}$  and  $3.4e^2\text{fm}^4$  in  $^{40}\text{Mg}$  [51]. Hindrance of the proton excitation in drip-line nuclei is due to the extreme spatial extension of neutron wave functions and decoupling with proton wave functions [51].

The discussion for enhancement of the quadrupole transition strength to the low-lying  $K^\pi = 0^+$  mode is also applicable to the pair transition strength. In the middle and right panels of Fig. 3, we show two kinds of strength for neutron pair transitions; one is the monopole pair transition and another the quadrupole pair transition,

$$\hat{P}_{00}^\dagger = \int d\mathbf{r} \hat{\psi}^\dagger(\mathbf{r} \uparrow) \hat{\psi}^\dagger(\mathbf{r} \downarrow), \quad (10a)$$

$$\hat{P}_{20}^\dagger = \int d\mathbf{r} r^2 Y_{20}(\hat{r}) \hat{\psi}^\dagger(\mathbf{r} \uparrow) \hat{\psi}^\dagger(\mathbf{r} \downarrow). \quad (10b)$$

For the quadrupole pair transitions, we see a prominent peak at 1.37 MeV, whereas no peak is seen at this energy for the monopole pair transitions. The origin of this contrasting behavior is understood as follows: The quadrupole (monopole) pairing matrix elements for individual 2qp excitations are in opposite phase (in phase) between the down-sloping prolate levels and the up-sloping oblate levels. As the transition matrix elements for the QRPA eigenmodes are determined by the similar way for the p-h transition matrix elements (See Eq. (B4)), they contribute coherently and destructively for the quadrupole and monopole pair transitions, respectively. As a consequence, the quadrupole-pair transition strength to the lowest  $K^\pi = 0^+$  collective excited state is greatly enhanced, whereas the monopole-pair transition strength to this state almost vanishes.

Therefore, in a deformed system where the up- and down-sloping orbitals exist near the Fermi level and the pairing fluctuation becomes important, we can expect the emergence of the low-lying mode which has extremely enhanced strengths both for the quadrupole p-h and for

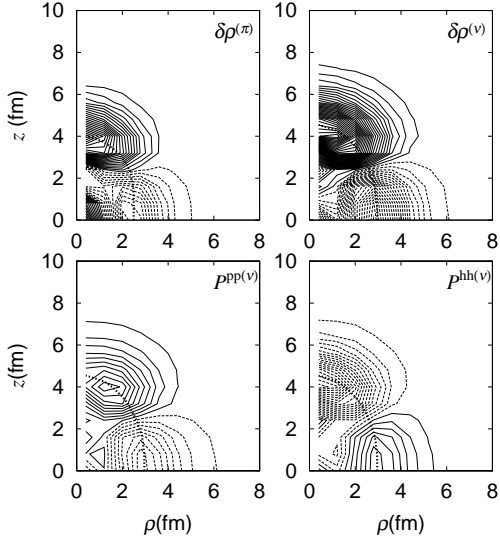


FIG. 5: Transition densities to the  $K^\pi = 0^+$  state at 1.37 MeV. The particle-hole transition densities of protons and neutrons (upper panels), the particle-particle and hole-hole transition densities of neutrons (lower panels). Solid and dashed lines indicate positive and negative transition densities, and the contour lines are plotted at intervals of  $3 \times 10^{-4} \text{ fm}^{-3}$ . The thick dotted lines denote the proton and neutron half densities,  $0.041$  and  $0.049 \text{ fm}^{-3}$ , respectively.

the quadrupole p-p (pair) transition.

The low-lying  $K^\pi = 0^+$  modes possibly emerge both in stable and in unstable deformed nuclei, and the unique feature in neutron-rich nuclei is that they are mainly generated by neutrons, whose wave functions have spatially extended structure due to the shallow Fermi level. In order to see the unique spatial structure, we show in Fig. 5 three kinds of transition densities;

$$\delta \rho^{(\tau)}(\rho, z) = \langle \lambda | \sum_{\sigma} \psi_{\tau}^{\dagger}(\rho, z, \sigma) \psi_{\tau}(\rho, z, \sigma) | 0 \rangle, \quad (11a)$$

$$P^{pp(\nu)}(\rho, z) = \langle \lambda | \psi_{\nu}^{\dagger}(\rho, z, \uparrow) \psi_{\nu}^{\dagger}(\rho, z, \downarrow) | 0 \rangle, \quad (11b)$$

$$P^{hh(\nu)}(\rho, z) = \langle \lambda | \psi_{\nu}(\rho, z, \downarrow) \psi_{\nu}(\rho, z, \uparrow) | 0 \rangle, \quad (11c)$$

where they are called the p-h transition density, the p-p (particle-pair) transition density, and the h-h (hole-pair) transition density, respectively [27]. The upper panels show a typical shape vibration of protons and neutrons along the symmetry axis ( $z$ -axis). We can clearly see the spatial extension of the neutron wave functions; the excitation takes place in the skin region around 7–8 fm. This spatial extension of the neutron wave functions brings about the enhancement of the transition strength. Another unique feature of the low-lying  $K^\pi = 0^+$  mode is that the particle-pair and hole-pair transition densities have an appreciable amplitude and are almost comparable to the p-h transition density.

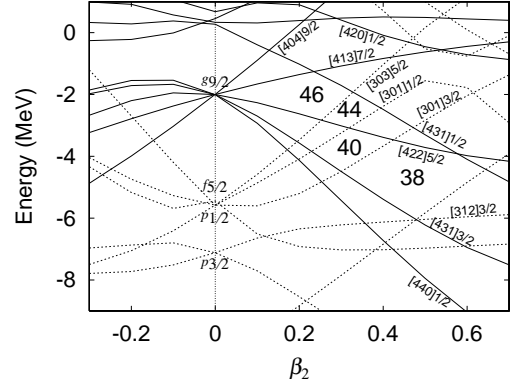


FIG. 6: Same as Fig. 1 but in  $^{64}\text{Cr}$ .

### B. Cr and Fe isotopes around $N = 40$

The deformation region near the shell closure gives a favorable situation for emergence of the soft  $K^\pi = 0^+$  modes discussed in the previous subsection because many orbitals with opposite quadrupole moments are crossing around the Fermi level. Since the low-lying  $K^\pi = 0^+$  mode is quite sensitive to the pairing correlation and deformation, we investigate in the present subsection the low-frequency  $K^\pi = 0^+$  excitations in neutron-rich Cr and Fe isotopes in  $N = 40$  region, and show generic features of the soft  $K^\pi = 0^+$  modes in deformed neutron-rich nuclei.

In a prolate deformation region around  $\beta_2 \simeq 0.3$ , deformed shell gaps associated with different  $\beta_2$  values appear at various neutron numbers due to the crossings between the down-sloping  $\nu[440]1/2$ ,  $\nu[431]3/2$  and  $\nu[431]1/2$  levels and the up-sloping  $\nu[301]3/2$ ,  $\nu[301]1/2$  and  $\nu[303]5/2$  levels (see Fig. 6).

According to the Skyrme HFB calculations [61, 62], the ground state of the neutron-rich Cr and Fe isotopes with  $N \simeq 40$  has a finite deformation around  $\beta_2 = 0.3$ .

The top panels in Fig. 7 show the isoscalar quadrupole transition strengths for the  $K^\pi = 0^+$  excitations. We can see a prominent peak at around 1 MeV in all nuclei under consideration. All low-lying states obtained here have extremely enhanced transition strengths (note that 1 W. u. is  $14.6\text{--}17.1 \text{ fm}^4$  for  $^{62\text{--}70}\text{Cr}$  and  $15.2\text{--}17.8 \text{ fm}^4$  for  $^{64\text{--}72}\text{Fe}$ ). These excitation modes are generated by coherent superposition of neutron 2qp excitations among the up- and the down-sloping levels as in  $^{34}\text{Mg}$ .

Furthermore, we can see an interesting feature from this systematic calculation; the transition strengths become enhanced at  $N = 38$  and  $46$ , and are symmetric at  $N = 42$ . This feature can be understood by the role of the  $\Omega^\pi = 1/2^+$  levels. In  $^{62}\text{Cr}$  and  $^{64}\text{Fe}$ , 2qp excitations of the up-sloping  $(\nu[301]3/2)^2$  and the down-sloping  $(\nu[440]1/2)^2$  have largest contributions to the lowest  $K^\pi = 0^+$  state. The transition strength of the  $(\nu[440]1/2)^2$  excitation is  $86 \text{ fm}^4$  (5.9 W.u.) in  $^{62}\text{Cr}$  and  $64 \text{ fm}^4$  (4.2 W.u.) in  $^{64}\text{Fe}$ , whereas that of the

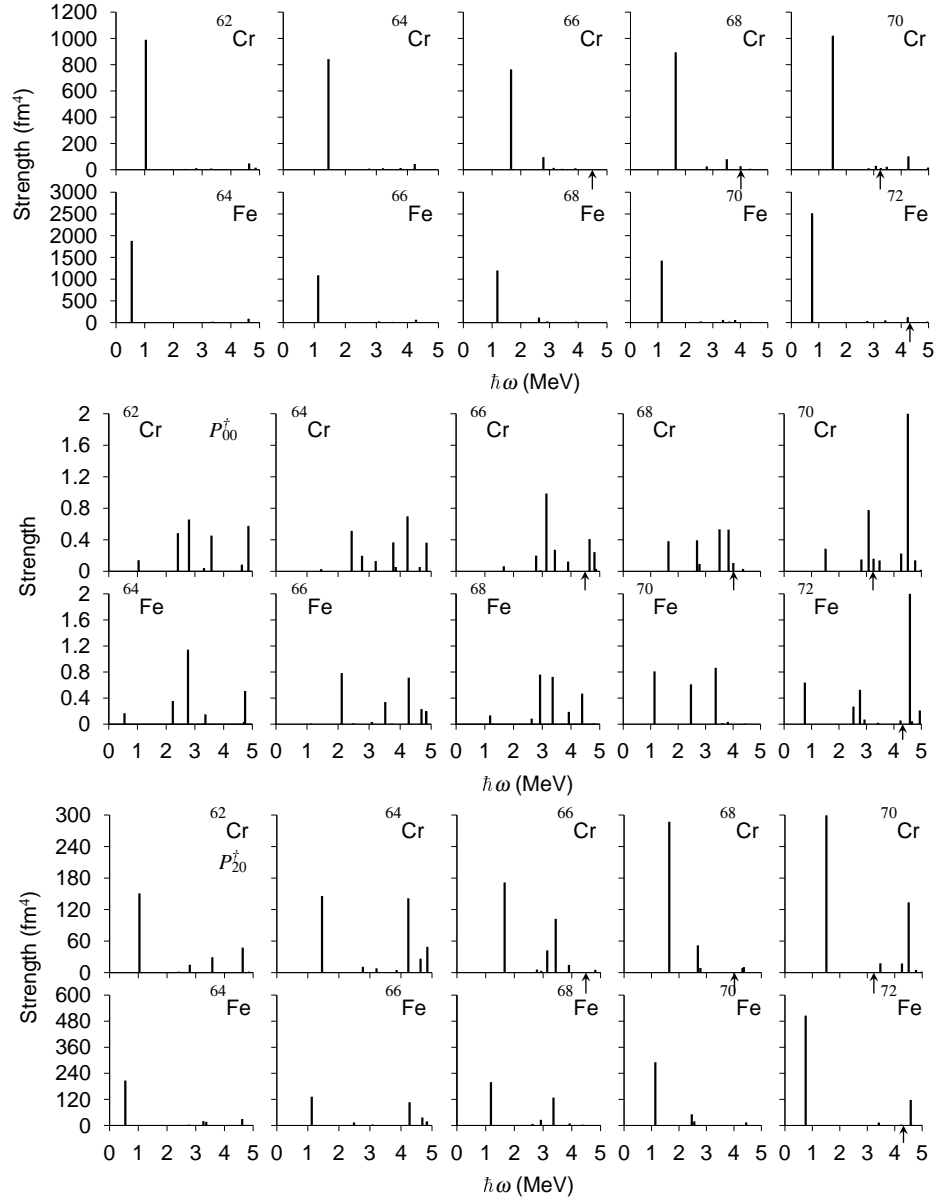


FIG. 7: Isoscalar quadrupole (top), the monopole-pair (middle), and the quadrupole-pair (bottom) transition strengths for the  $K^\pi = 0^+$  excitations in  $^{62-70}\text{Cr}$  and  $^{64-72}\text{Fe}$  obtained by the QRPA calculations using  $\beta_2 = 0.3$  and  $V_0 = -420 \text{ MeV}\cdot\text{fm}^3$ . The self-consistent factors are  $f_{ph}=0.72-0.74$  and  $f_{pp} = 1.43$  for Cr isotopes, and  $f_{ph}=0.74-0.79$  and  $f_{pp}=1.39-1.42$  for Fe isotopes. The arrows denote the neutron threshold energies.

$(\nu[301]3/2)^2$  is  $9.6 \text{ fm}^4$  and  $8.6 \text{ fm}^4$ , respectively. This indicates the  $\nu[440]1/2$  level has a spatially extended structure (in  $^{62}\text{Cr}$ , the root-mean-square radius of the  $\nu[440]1/2$  level is  $5.1 \text{ fm}$ , whereas the total neutron r.m.s. radius is  $4.2 \text{ fm}$ ). As the neutron number increases, the transition strength decreases as a consequence of the decreasing contribution of the  $(\nu[440]1/2)^2$  excitation.

As the neutron number approaches  $N = 46$ , the  $\nu[431]1/2$  level becomes close to the Fermi surface (see Fig. 6). In  $^{70}\text{Cr}$  and  $^{72}\text{Fe}$ , 2qp excitations of the up-sloping  $(\nu[303]5/2)^2$  and the down-sloping  $(\nu[431]1/2)^2$

have largest contributions to the lowest  $K^\pi = 0^+$  state. The transition strength of the  $(\nu[431]1/2)^2$  excitation is  $115 \text{ fm}^4$  ( $6.7 \text{ W.u.}$ ) in  $^{70}\text{Cr}$  and  $95 \text{ fm}^4$  ( $5.4 \text{ W.u.}$ ) in  $^{72}\text{Fe}$ . This 2qp transition strength becomes large because of the shallower Fermi level and the spatially extended structure of the quasiparticle wave function of the  $\nu[431]1/2$  level.

At  $N = 42$ , both of the  $\nu[440]1/2$  and the  $\nu[431]1/2$  levels are located far from the Fermi level, and 2qp excitations of the  $(\nu[301]1/2)^2$  and the  $(\nu[422]5/2)^2$  have main contributions to the lowest  $K^\pi = 0^+$  state in  $^{66}\text{Cr}$  and  $^{68}\text{Fe}$ . These quadrupole transition matrix elements

have opposite signs, but these transition strengths are less than 1 W.u.

In Fig. 7, we show also the strengths for the monopole- and quadrupole-pair transitions. As in  $^{34}\text{Mg}$ , these low-lying  $K^\pi = 0^+$  modes have enhanced strengths for the quadrupole pair transition, whereas disappearing strengths for the monopole pair transition. This systematic calculation shows an importance of the dynamical pairing: Fluctuation of the pairing field, which is deformed as well as the mean field, is crucial for generating the collective  $K^\pi = 0^+$  modes.

#### IV. SUMMARY

We have studied low-frequency  $K^\pi = 0^+$  modes in neutron-rich nuclei, taking account of the effects of nuclear deformation, pairing correlation and continuum coupling simultaneously. New type of this excitation mode is generated by coherent superposition of neutron 2qp excitations near the Fermi level whose wave functions have spatially extended structure. It is found that the dynamical pairing correlation, *i.e.*, the pairing vibration enhances its collectivity.

In the spherical neutron-rich nuclei, the effect of the dynamical pairing has been investigated in detail in Refs. [23, 27, 32]. We have shown in this paper the importance of the dynamical pairing in neutron-rich deformed systems. In a deformed system where the up- and down-sloping orbitals exist near the Fermi level, one obtains the low-lying mode possessing extremely enhanced strengths both for the quadrupole p-h transition and for the quadrupole p-p (pair) transition induced by the pairing fluctuation.

We found that the coupling between the pairing vibration and the neutron-skin vibration brings forth the soft  $K^\pi = 0^+$  mode in deformed Mg region with  $N = 22$ . Furthermore, it was shown that emergence of low-lying  $K^\pi = 0^+$  modes is not restricted in the neutron-rich Mg isotopes. As an example, in neutron-rich Cr and Fe isotopes around  $N = 40$ , we showed that the coherent coupling between the pairing vibration and the  $\beta$ -vibration of the neutron skin brings about the striking enhancement of the strengths for the quadrupole p-h and the quadrupole pair transition.

#### Acknowledgments

The authors thank K. Matsuyanagi for valuable comments and discussions. They also acknowledge N. Van Giai for useful discussions. One of the authors (K.Y) is supported by Research Fellowships of the Japan Society for the Promotion of Science for Young Scientists. The numerical calculations were performed on the NEC SX-8 supercomputers at Yukawa Institute for Theoretical Physics, Kyoto University and at Research Center for Nuclear Physics, Osaka University.

#### APPENDIX A: MATRIX ELEMENTS FOR ONE-BODY OPERATORS

Let us first consider matrix elements for particle-hole type one-body operators

$$\langle ab | \hat{O}_K^{(uv)} | \text{HFB} \rangle, \quad (\text{A1})$$

where

$$\hat{O}_K^{(uv)} = \sum_{\sigma\sigma'} \int d\mathbf{r} d\mathbf{r}' \delta_{\sigma,\sigma'} \delta(\mathbf{r} - \mathbf{r}') O_K^{(uv)}(\mathbf{r}) \hat{\psi}^\dagger(\mathbf{r}'\sigma') \hat{\psi}(\mathbf{r}\sigma), \quad (\text{A2})$$

and the HFB ground state and the 2qp excited states

$$\hat{\beta}_i | \text{HFB} \rangle = 0, \quad (\text{A3a})$$

$$|ab\rangle = \hat{\beta}_a^\dagger \hat{\beta}_b^\dagger | \text{HFB} \rangle \quad (\text{A3b})$$

are described by the quasiparticle operators. These operators are defined by the generalized Bogoliubov transformation

$$\hat{\psi}^\dagger(\mathbf{r}\sigma) = \sum_k \varphi_{1,k}(\mathbf{r}\bar{\sigma}) \hat{\beta}_k^\dagger + \varphi_{2,k}^*(\mathbf{r}\sigma) \hat{\beta}_k, \quad (\text{A4a})$$

$$\hat{\psi}(\mathbf{r}\sigma) = \sum_k \varphi_{1,k}^*(\mathbf{r}\bar{\sigma}) \hat{\beta}_k + \varphi_{2,k}(\mathbf{r}\sigma) \hat{\beta}_k^\dagger, \quad (\text{A4b})$$

where

$$\varphi_k(\mathbf{r}\bar{\sigma}) = -2\sigma\varphi_k(\mathbf{r} - \sigma). \quad (\text{A5})$$

In Appendices, we omit the subscript  $\tau$  for simplicity.

The 2qp transition matrix elements are calculated as

$$\begin{aligned} & \langle ab | \hat{O}_K^{(uv)} | \text{HFB} \rangle \\ &= \langle \text{HFB} | \hat{\beta}_b \hat{\beta}_a \hat{O}_K^{(uv)} | \text{HFB} \rangle \\ &= \sum_{kk'} \sum_{\sigma\sigma'} \int d\mathbf{r} d\mathbf{r}' \delta_{\sigma,\sigma'} \delta(\mathbf{r} - \mathbf{r}') O_K^{(uv)}(\mathbf{r}) \\ & \quad \times \varphi_{1,k}(\mathbf{r}'\bar{\sigma}') \varphi_{2,k'}(\mathbf{r}\sigma) \langle \text{HFB} | \hat{\beta}_b \hat{\beta}_a \hat{\beta}_k^\dagger \hat{\beta}_{k'}^\dagger | \text{HFB} \rangle \\ &= \int d\mathbf{r} O_K^{(uv)}(\mathbf{r}) \{ -\varphi_{1,a}(\mathbf{r}\downarrow) \varphi_{2,b}(\mathbf{r}\uparrow) + \varphi_{1,a}(\mathbf{r}\uparrow) \varphi_{2,b}(\mathbf{r}\downarrow) \\ & \quad + \varphi_{1,b}(\mathbf{r}\downarrow) \varphi_{2,a}(\mathbf{r}\uparrow) - \varphi_{1,b}(\mathbf{r}\uparrow) \varphi_{2,a}(\mathbf{r}\downarrow) \} \\ &\equiv O_{K,ab}^{(uv)} \end{aligned} \quad (\text{A6})$$

using the quasiparticle wave functions, and we employed the Wick's theorem. In the cylindrical coordinate representation, we can rewrite as

$$\begin{aligned} & \langle ab | \hat{O}_K^{(uv)} | \text{HFB} \rangle = \\ & 2\pi \delta_{K,\Omega_a+\Omega_b} \int \rho d\rho dz O_K^{(uv)}(\rho, z) \\ & \quad \times \{ \varphi_{1,a}(\rho, z, \uparrow) \varphi_{2,b}(\rho, z, \downarrow) - \varphi_{1,a}(\rho, z, \downarrow) \varphi_{2,b}(\rho, z, \uparrow) \\ & \quad - \varphi_{1,b}(\rho, z, \uparrow) \varphi_{2,a}(\rho, z, \downarrow) + \varphi_{1,b}(\rho, z, \downarrow) \varphi_{2,a}(\rho, z, \uparrow) \}, \end{aligned} \quad (\text{A7})$$

where

$$O_K^{(uv)}(\rho, z) = O_K^{(uv)}(\mathbf{r})e^{iK\phi}. \quad (\text{A8})$$

Next we consider the pair creation operators consisting of nucleons with opposite direction of spins

$$\hat{O}_K^{(uu)} = \int d\mathbf{r} d\mathbf{r}' \delta(\mathbf{r} - \mathbf{r}') O_K^{(uu)}(\mathbf{r}) \hat{\psi}^\dagger(\mathbf{r}' \uparrow) \hat{\psi}^\dagger(\mathbf{r} \downarrow). \quad (\text{A9})$$

The matrix elements read

$$\begin{aligned} & \langle ab | \hat{O}_K^{(uu)} | \text{HFB} \rangle \\ &= \langle \text{HFB} | \hat{\beta}_b \hat{\beta}_a \hat{O}_K^{(uu)} | \text{HFB} \rangle \\ &= \sum_{kk'} \int d\mathbf{r} d\mathbf{r}' \delta(\mathbf{r} - \mathbf{r}') O_K^{(uu)}(\mathbf{r}) \\ & \quad \times \varphi_{1,k}(\mathbf{r}' \uparrow) \varphi_{1,k'}(\mathbf{r} \downarrow) \langle \text{HFB} | \hat{\beta}_b \hat{\beta}_a \hat{\beta}_k^\dagger \hat{\beta}_{k'}^\dagger | \text{HFB} \rangle \\ &= \int d\mathbf{r} O_K^{(uu)}(\mathbf{r}) \{ -\varphi_{1,a}(\mathbf{r} \downarrow) \varphi_{1,b}(\mathbf{r} \uparrow) + \varphi_{1,b}(\mathbf{r} \downarrow) \varphi_{1,a}(\mathbf{r} \uparrow) \} \\ &= 2\pi \delta_{K, \Omega_a + \Omega_b} \int \rho d\rho dz O_K^{(uu)}(\rho, z) \\ & \quad \times \{ \varphi_{1,a}(\rho, z, \uparrow) \varphi_{1,b}(\rho, z, \downarrow) - \varphi_{1,a}(\rho, z, \downarrow) \varphi_{1,b}(\rho, z, \uparrow) \}, \end{aligned} \quad (\text{A10})$$

where

$$O_K^{(uu)}(\rho, z) = O_K^{(uu)}(\mathbf{r})e^{iK\phi}. \quad (\text{A11})$$

## APPENDIX B: QRPA TRANSITION MATRIX ELEMENTS

In terms of the nucleon annihilation and creation operators in the coordinate representation, the quadrupole operator is represented as

$$\hat{Q}_{2K} = \sum_{\sigma} \int d\mathbf{r} r^2 Y_{2,-K}(\hat{r}) \hat{\psi}^\dagger(\mathbf{r}\sigma) \hat{\psi}(\mathbf{r}\sigma). \quad (\text{B1})$$

The intrinsic matrix elements  $\langle \lambda | \hat{Q}_{2K} | 0 \rangle$  of the quadrupole operator between the excited state  $|\lambda\rangle$  and the ground state  $|0\rangle$  are given by

$$\langle \lambda | \hat{Q}_{2K} | 0 \rangle = \sum_{ab} Q_{2K,ab}^{(uv)} (f_{ab}^\lambda + g_{ab}^\lambda) = \sum_{ab} M_{2K,ab}^{(uv)}, \quad (\text{B2})$$

where

$$Q_{2K,ab}^{(uv)} = \langle ab | \hat{Q}_{2K} | \text{HFB} \rangle \quad (\text{B3})$$

calculated by using the quasiparticle wave-functions as (A7).

We can furthermore calculate the intrinsic matrix element of the pair creation operator as

$$\begin{aligned} \langle \lambda | \hat{P}_0^\dagger | 0 \rangle &= \sum_{ab} (f_{ab}^\lambda P_{00,ab}^{(uu)} + g_{ab}^\lambda P_{00,ab}^{(vv)}) = \sum_{ab} M_{00,ab}^{(\text{add})}, \\ \langle \lambda | \hat{P}_{2K}^\dagger | 0 \rangle &= \sum_{ab} (f_{ab}^\lambda P_{2K,ab}^{(uu)} + g_{ab}^\lambda P_{2K,ab}^{(vv)}) = \sum_{ab} M_{2K,ab}^{(\text{add})}, \end{aligned} \quad (\text{B4a})$$

$$(\text{B4b})$$

where the monopole- and quadrupole-pair creation operators are defined by Eq.(10). The matrix element of 2qp excitation  $P_{00,ab}^{(uu)}$ ,  $P_{00,ab}^{(vv)}$ ,  $P_{2K,ab}^{(uu)}$  and  $P_{2K,ab}^{(vv)}$  are given by (A10) and by the similar expression for  $\hat{O}_K^{(vv)}$ .

## APPENDIX C: CALCULATION OF THE MOMENT OF INERTIA

We estimate moments of inertia using the spurious solution of the RPA equation [14]

$$\begin{pmatrix} A & B \\ B^* & A^* \end{pmatrix}_{\alpha\beta\gamma\delta} \begin{pmatrix} J_x \\ -J_x^* \end{pmatrix}_{\gamma\delta} = 0, \quad (\text{C1a})$$

$$\begin{pmatrix} A & B \\ B^* & A^* \end{pmatrix}_{\alpha\beta\gamma\delta} \begin{pmatrix} \Theta \\ -\Theta^* \end{pmatrix}_{\gamma\delta} = \frac{\hbar}{i} \frac{1}{\mathcal{J}_{\text{TV}}} \begin{pmatrix} J_x \\ J_x^* \end{pmatrix}_{\alpha\beta}, \quad (\text{C1b})$$

where  $\hat{J}_x$  is the angular momentum operator consisting of the orbital part  $\hat{l}_x$  and the spin part  $\hat{s}_x$ , and its conjugate operator  $\hat{\Theta}$ .

The Thouless-Valatin moment of inertia  $\mathcal{J}_{\text{TV}}$  is determined thorough the orthonormal condition

$$(J_x^* \ J_x)_{\alpha\beta} \begin{pmatrix} \Theta \\ -\Theta^* \end{pmatrix}_{\gamma\delta} = \frac{\hbar}{i} \delta_{\alpha\beta, \gamma\delta}, \quad (\text{C2})$$

as

$$\mathcal{J}_{\text{TV}} = 2\hbar^2 \sum_{\alpha\beta\gamma\delta} (J_x)_{\alpha\beta}^* (A - B)_{\alpha\beta\gamma\delta}^{-1} (J_x)_{\gamma\delta}. \quad (\text{C3})$$

Turning off the residual interaction, we obtain the expression for the Inglis-Belyaev moment of inertia  $\mathcal{J}_{\text{Belyaev}}$

$$\mathcal{J}_{\text{Belyaev}} = 2\hbar^2 \sum_{\alpha\beta} \frac{|J_x|_{\alpha\beta}^2}{E_\alpha + E_\beta}. \quad (\text{C4})$$

- 
- [1] P. von Neumann-Cosel and T. Aumann (ed.), *Proceedings of the 2nd International Conference on Collective Motions in Nuclei under Extreme Conditions*, Nucl. Phys. **A788**, (2007).  
 [2] T. Motobayashi, *et al.*, Phys. Lett. **B349**, 9 (1995).

- [3] H. Iwasaki, *et al.*, Phys. Lett. **B522**, 227 (2001).  
 [4] K. Yoneda, *et al.*, Phys. Lett. **B499**, 233 (2001).  
 [5] J. A. Church, *et al.*, Phys. Rev. C **72**, 054320 (2005).  
 [6] Z. Elekes, *et al.*, Phys. Rev. C **73**, 044314 (2006).  
 [7] T. Baumann, *et al.*, Nature **449**, 1022 (2007).



- [8] T. Otsuka, Y. Utsuno, M. Honma, and T. Mizusaki, *Prog. Part. Nucl. Phys.* **46**, 155 (2001).
- [9] E. Caurier, F. Nowacki, A. Poves, *Nucl. Phys.* **A742**, 14 (2004).
- [10] J. Terasaki, H. Flocard, P.-H. Heenen, and P. Bonche, *Nucl. Phys.* **A621**, 706 (1997).
- [11] R. Rodríguez-Guzmán, J. L. Egido, L. M. Robledo, *Nucl. Phys.* **A709**, 201 (2002).
- [12] P.-G. Reinhard, D. J. Dean, W. Nazarewicz, J. Dobaczewski, J. A. Maruhn, M. R. Strayer, *Phys. Rev. C* **60**, 014316 (1999) and references therein.
- [13] S. G. Nilsson and I. Ragnarsson, *Shapes and Shells in Nuclear Structure*, (Cambridge University Press, 1995).
- [14] P. Ring and P. Schuck, *The Nuclear Many-Body Problem* (Springer, 1980).
- [15] M. Hannawald *et al.*, *Phys. Rev. Lett.* **82**, 1391 (1999).
- [16] O. Sorlin *et al.*, *Nucl. Phys.* **A660**, 3 (1999).
- [17] O. Sorlin *et al.*, *Eur. Phys. J. A.* **16**, 55 (2003).
- [18] S. Lunardi *et al.*, *Phys. Rev. C* **76**, 034303 (2007).
- [19] E. Caurier, F. Nowacki, and A. Poves, *Eur. Phys. J. A.* **15**, 145 (2002).
- [20] I. Hamamoto, H. Sagawa and X. Z. Zhang, *Phys. Rev. C* **53**, 765 (1996); *ibid.* **55**, 2361 (1997); *ibid.* **56**, 3121 (1997); *ibid.* **57**, R1064 (1998); *ibid.* **64**, 024313 (2001).
- [21] I. Hamamoto and H. Sagawa, *Phys. Rev. C* **60**, 064314 (1999); *ibid.* **62**, 024319 (2000); *ibid.* **66**, 044315 (2002).
- [22] S. Shlomo and B. Agrawal, *Nucl. Phys.* **A722**, 98c (2003).
- [23] M. Matsuo, *Nucl. Phys.* **A696**, 371 (2001).
- [24] K. Hagino, H. Sagawa, *Nucl. Phys.* **A695**, 82 (2001).
- [25] E. Khan, N. Sandulescu, M. Grasso, N. Van Giai, *Phys. Rev. C* **66**, 024309 (2002).
- [26] M. Yamagami, N. Van Giai, *Phys. Rev. C* **69**, 034301 (2004).
- [27] M. Matsuo, K. Mizuyama, Y. Serizawa, *Phys. Rev. C* **71**, 064326 (2005).
- [28] J. Terasaki, J. Engel, M. Bender, J. Dobaczewski, W. Nazarewicz, M. Stoitsov, *Phys. Rev. C* **71**, 034310 (2005) and references therein.
- [29] J. Terasaki, J. Engel, *Phys. Rev. C* **74**, 044301 (2006).
- [30] K. Mizuyama, M. Matsuo, Y. Serizawa, *arXiv:0706.1115*.
- [31] D. Vretenar, N. Paar, P. Ring, G. A. Lalazissis, *Nucl. Phys.* **A692**, 496 (2001).
- [32] N. Paar, P. Ring, T. Nikšić, D. Vretenar, *Phys. Rev. C* **67**, 034312 (2003).
- [33] N. Paar, T. Nikšić, D. Vretenar, P. Ring, *Phys. Rev. C* **69**, 054303 (2004).
- [34] N. Paar, T. Nikšić, D. Vretenar, P. Ring, *Phys. Lett.* **B606**, 288 (2005).
- [35] L. G. Cao, Z. Y. Ma, *Phys. Rev. C* **71**, 034305 (2005).
- [36] G. Giambrone, S. Scheit, F. Barranco, P. F. Bortignon, G. Colò, D. Sarchi, E. Vigezzi, *Nucl. Phys.* **A726**, 3 (2003).
- [37] D. Sarchi, P. F. Bortignon, G. Colò, *Phys. Lett.* **B601**, 27 (2004).
- [38] S. Péru, J. F. Berger, P. F. Bortignon, *Eur. Phys. J. A* **26**, 25 (2005).
- [39] K. Yoshida, M. Yamagami, K. Matsuyanagi, *Prog. Theor. Phys.* **113**, 1251 (2005).
- [40] T. Nakatsukasa and K. Yabana, *Phys. Rev. C* **71**, 024301 (2005).
- [41] A. Muta, J.-I. Iwata, Y. Hashimoto, and K. Yabana, *Prog. Theor. Phys.* **108**, 1065 (2002).
- [42] H. Imagawa and Y. Hashimoto, *Phys. Rev. C* **67**, 037302 (2003).
- [43] T. Inakura, H. Imagawa, Y. Hashimoto, S. Mizutori, M. Yamagami and K. Matsuyanagi, *Nucl. Phys.* **A768**, 61 (2006).
- [44] P. Urkedal, X. Z. Zhang and I. Hamamoto, *Phys. Rev. C* **64**, 054304 (2001).
- [45] K. Hagino, N. Van Giai and H. Sagawa, *Nucl. Phys.* **A731**, 264 (2004).
- [46] S. Péru, H. Goutte, J. F. Berger, *Nucl. Phys.* **A788**, 44c (2007).
- [47] D. Peña Arteaga, and P. Ring, *Prog. Part. Nucl. Phys.* **59**, 314 (2007).
- [48] T. Nakatsukasa, T. Inakura, K. Yabana, *Phys. Rev. C* **76**, 024318 (2007).
- [49] K. Yoshida, N. Van Giai, *arXiv:0802.1687*.
- [50] J. Dobaczewski, H. Flocard and J. Treiner, *Nucl. Phys.* **A422**, 103 (1984).
- [51] K. Yoshida, M. Yamagami, K. Matsuyanagi, *Nucl. Phys.* **A779**, 99 (2006).
- [52] A. Bulgac, Preprint No. FT-194-1980, Institute of Atomic Physics, Bucharest, 1980. [*arXiv:nucl-th/9907088*]
- [53] E. Terán, V. E. Oberacker and A. S. Umar, *Phys. Rev. C* **67**, 064314 (2003).
- [54] G. F. Bertsch, H. Esbensen, *Ann. Phys.* **209**, 327 (1991).
- [55] J. Terasaki, P.-H. Heenen, P. Bonche, J. Dobaczewski, H. Flocard, *Nucl. Phys.* **A593**, 1 (1995).
- [56] D. J. Rowe, *Nuclear Collective Motion*, (Methuen and Co. Ltd., 1970).
- [57] S. Shlomo and G. F. Bertsch, *Nucl. Phys.* **A243**, 507 (1975).
- [58] L. M. Eisenberg and W. Greiner, *Nuclear Models*, vol. I (North Holland, 1970).
- [59] A. Bohr and B. R. Motteleson, *Nuclear Structure*, vol. II (Benjamin, 1975; World Scientific, 1998).
- [60] D. M. Brink and R. A. Broglia, *Nuclear Superfluidity, Pairing in Finite Systems* (Cambridge University Press, 2005).
- [61] M. V. Stoitsov, J. Dobaczewski, W. Nazarewicz, S. Pittel and D. J. Dean, *Phys. Rev. C* **68**, 054312 (2003).
- [62] M. V. Stoitsov, J. Dobaczewski, W. Nazarewicz, P. Ring, *Comp. Phys. Comm.* **167**, 43 (2005).